THE JOURNAL OF PHYSICAL CHEMISTRY C

Article

pubs.acs.org/JPCC

Small- and Wide-Angle X-ray Scattering Characterization of Bulk Heterojunction Polymer Solar Cells with Different Fullerene Derivatives

Yu-Ching Huang,[†] Cheng-Si Tsao,*[,†] Chih-Min Chuang,[†] Chia-Hsin Lee,[†] Fan-Hsuan Hsu,[†] Hou-Chin Cha,[†] Charn-Ying Chen,[†] Tsung-Han Lin,[‡] Chun-Jen Su,[§] U-Ser Jeng,[§] and Wei-Fang Su*[,‡]

[†]Institute of Nuclear Energy Research, Longtan, Taoyaun 32546, Taiwan

[‡]Department of Materials Science and Engineering, National Taiwan University, Taipei 10617, Taiwan

[§]National Synchrotron Radiation Research Center, Hsinchu 30077, Taiwan

Supporting Information

ABSTRACT: The aim of this study is to quantitatively investigate the effect of different fullerene type ($PC_{60}BM$ and $PC_{70}BM$) on various morphological structures and power conversion efficiency (PCE) in the bulk heterojunction (BHJ) P3HT/PC_xBM solar cells. The solar cells are fabricated by spin coating without thermal annealing. The quantitative investigations of three-dimensional self-organized nanostructures are performed by using combined grazing-incidence small- and wide-angle X-ray scattering technique (GISAXS/GIWAXS). Two types of nanostructures are observed due to the phase separation in the BHJ films during the processing. They include (1) intercalated PC_xBM molecules around boundary of P3HT crystalline domain and within amorphous domain and (2) aggregated PC_xBM clusters in PC_xBM domains. The lamellar spacing of P3HT crystalline domains in P3HT/$PC_{70}BM$ is larger than that in P3HT/$PC_{60}BM$. This result indicates more interfacial areas are generated between $PC_{70}BM$ and P3HT at the molecular scale for more efficient charge separation. On the other hand, the size, volume fraction, partial attachment, and spatial distribution of $PC_{60}BM$ clusters are larger than that of $PC_{70}BM$ clusters, which reveals more efficient electron transport in P3HT/$PC_{60}BM$. We deduce the correlation between nanostructures and PCE (3.25% and 2.64%, respectively, for P3HT/$PC_{70}BM$ and P3HT/$PC_{60}BM$). The structure of fullerene intercalated with P3HT rather than the size of fullerene cluster plays a major role in the PCE performance of BHJ solar cell without thermal annealing.

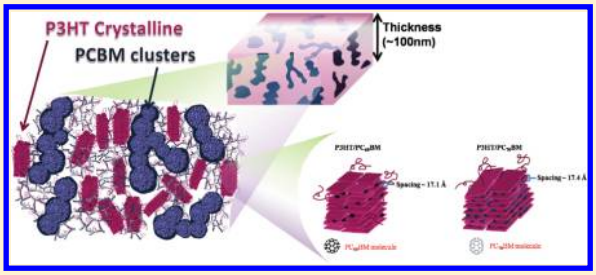

INTRODUCTION

Bulk heterojunction (BHJ) polymer solar cells have attracted broad attention due to the commercial potential of large area, low manufacturing cost, and solution process.[1−3] Poly(3-hexylthiophene) (P3HT) is the most widely used polymer donor in BHJ polymer solar cells. The [6,6]-phenyl-C_{61}-butyric acid methyl ester ($PC_{60}BM$, fullerene derivative) is a representative acceptor. The PCE of P3HT/$PC_{60}BM$ as the active layer of BHJ polymer solar cell has reached over 4%.[4,5] Previous research has demonstrated that the power conversion efficiency (PCE) critically depends on the three-dimensional (3D) self-organized nanostructure of the active layer.[6−8] This nanostructure is mainly resulted from the phase separation of P3HT/$PC_{60}BM$ blend.[9] An interpenetrating (bicontinuous) network of phase-separated nanodomains is formed for effective transport of electron and hole to their respective electrodes. The self-assembled nanostructure can be manipulated by thermal or solvent annealing for improving PCE.[10−12] However, how the self-organized nanostructure can be tuned by the processing and the type of material is not fully understood at present. Previous studies have noted the role of phase-separated individual nanodomains (e.g., aggregated PCBM cluster and P3HT crystallite) in the performance improvement of BHJ solar cells.[13−18]

On the other hand, recent studies have tuned the properties of the BHJ polymer solar cells by adjusting fullerene size to control intercalation.[19,20] The increase of lamellar spacing inside polymer crystallite due to the intercalation of fullerene between side chains of polymer was revealed by X-ray diffraction measurement. It leads to a significant increase in the donor−acceptor interfacial area and thus better photoluminescence (PL) quenching (better separation of charges).[20] It can be regarded as intimate mixing of polymer and fullerene on a molecular scale in the intercalated phase. These studies used the fullerene intercalation as a design parameter of new BHJ polymer solar cell. However, the quantitative analysis regarding the phase-separated nanoscale domains of donor and acceptor phases (i.e., the interpenetrating network as the paths for transporting charges) was lacking. The correlation between the intercalation and improvement of PCE was not established.

Received: October 22, 2011
Revised: April 4, 2012
Published: April 11, 2012

Thus, comprehensive investigations from phase-separated nanodomains to molecular intercalation of fullerene are needed to enable the fully understanding of how the role of intercalation affects the PCE. Recently, small-angle X-ray scattering technique (SAXS) has been used as a powerful tool to characterize the overall 3D nanostructure of thin film samples.[15−17,21] As compared with the conventional tools, such as transmission electron microscopy (TEM) and atomic force microscopy (AFM), SAXS is not limited on the localized nanostructure characterization.

Over the past years, an interesting fullerene derivative, [6,6]-phenyl-C_{71}-butyric acid methyl ester ($PC_{70}BM$), has been used in the BHJ polymer solar cells with high PCE.[22−24] The $PC_{70}BM$ exhibits better absorption behavior in the wavelength regions from 350 to 500 nm than $PC_{60}BM$.[22,25] It has been reported that P3HT absorption is dominant, and the contribution of $PC_{70}BM$ absorption is insufficient in P3HT/$PC_{70}BM$ solar cells before thermal treatment.[26] Therefore, it is fundamentally important to explore how the self-organized nanostructure of the BHJ film is tuned by $PC_{60}BM$ and $PC_{70}BM$ during the solvent evaporation process to improve the efficiency of solar cell.

In the present study, we prepared P3HT/$PC_{60}BM$ and P3HT/$PC_{70}BM$ solar cells by the slow-drying casting process using the high boiling point of 1,2-dichlorobenzene (DCB). Notably, the compatibility of $PC_{70}BM$ and P3HT in DCB is better than that of $PC_{60}BM$ and P3HT.[27] We employed both grazing-incidence small-angle and wide-angle X-ray scattering (GISAXS/GIWAXS) to quantitatively characterize (1) the size, volume fraction, and spatial distribution of aggregated PC_xBM cluster, (2) the size and internal spacing of lamellae of P3HT crystallite intercalated by PC_xBM molecules, and (3) the network structure of PC_xBM molecules dispersed in amorphous P3HT chains. The effect of different fullerene derivatives on the formation of various phase-separated nanostructures during the solvent evaporation is investigated here. The result also reveals the crystalline behavior of P3HT during phase separation is affected by the addition of different fullerene derivatives as compared to the crystalline behavior of pristine P3HT film. Also, the different characteristics of fullerene derivatives significantly affect the induction of distinctive aggregation and the spatial distribution of PC_xBM clusters. The transformation of PC_xBM clusters is closely related to the amount of PC_xBM molecules inside the P3HT. Furthermore, the correlation between various nanostructures and the performance of BHJ solar cells without thermal annealing is also discussed. The PCE value of P3HT/PCBM solar cells without thermal annealing is generally around 1%.[9,28,29] However, few devices can achieve up to 2.64%.[30] Rare studies correlated the PCE with nanostructure for these cells. In the present study, the PCE of BHJ polymer solar cell is improved up to 3.25% by adjusting different fullerenes without thermal annealing. We suggest that the P3HT-related structure may very likely play a major role in the performance of solar cells without thermal annealing. Furthermore, many researches have demonstrated that the intercalation of PCBM with polymer is a critical factor to achieve high PCE of BHJ solar cell due to the effective exciton dissociation at the interface between donor and acceptor in molecular scale.[19,20] Our study would further show that the increasing photocurrent of P3HT/$PC_{70}BM$ solar cell is attributed to the effective charge separation rather than the improved charge transport. The knowledge obtained here would be one of the keys into the rational design of high PCE BHJ solar cell (starting from the modification of fullerene derivative to the tuned nanostructures, thus improving PCE).

EXPERIMENTAL SECTION

In this experiment, the solution of P3HT and fullerene derivatives were prepared by blending the P3HT (M_w = 61 881 g mol^{-1}; PDI = 1.48; and RR = 97.2%; synthesized by Industrial Technology Research Institute, Hsinchu, Taiwan) and fullerene derivatives ($PC_{60}BM$ and $PC_{70}BM$, Aldrich) in a weight ratio of 1:1 dissolved in DCB according to literature.[31] The solution was stirred for overnight at 45 °C in a glovebox filled with N_2. These thin films for GISAXS and GIWAXS experiments were deposited on cleaned silicon wafers by spin coating at 800 rpm for 60 s. The structure of P3HT/PC_xBM thin film is unaffected by the use of different substrates (silicon wafers vs ITO/PEDOT−PSS, see Supporting Information, Figure S1). The thickness and area of the thin films are 100 nm and 2 cm × 1 cm, respectively. The simultaneous GISAXS and GIWAXS experiments were performed at the National Synchrotron Radiation Research Center, Taiwan. The GIWAXS and GISAXS intensities were simultaneously collected by a flat panel X-ray detector and a CCD detector, respectively. The scattered two-dimensional (2D) patterns were reduced to one-dimensional (1D) scattering profiles as a function of scattering vector Q. The details of scattering experiments, instrumental configuration, data reduction, and analysis model were described in our previous studies.[32,33] In this configuration, the out-of-plane direction is perpendicular to the substrate and thin film. The 1D GISAXS and GIWAXS profiles are mainly reduced along the out-of-plane and in-plane directions, respectively. The incident angle of the simultaneous GISAXS/GIWAXS measurements for each thin film sample was carefully aligned to be 0.2 ± 0.002°, for penetrating through the whole organic layer;[34] with the accuracy of the incidence, the sampling volumes (incidence-angle dependent) for all thin film samples were essentially the same within ±1.5%.

The absorption spectra of P3HT/PC_xBM thin films were measured by using UV−visible absorption spectroscopy (Perkin−Elmer Lambda 35). Two kinds of P3HT/PC_xBM thin films were measured in this study: one is deposited on a cleaned ITO glass from slow-drying (DCB as solvent) process, and the other is deposited from a relative fast-drying (chlorobenzene, CB as solvent) process. The absorption spectra were normalized to have equal film thickness. The film thickness was determined by a stylus profiler (AlphaStep D-100, KLA Tencor).

For solar cells, the active layer was deposited on the glass covered with ∼140 nm thick layers of indium tin oxide (ITO). The ITO glass substrate was cleaned by ultrasonic in a series of acetone and isopropanol. About a 40 nm thick layer of PEDOT−PSS (Baytron P, 4083) was spin coated to modify the surface of the ITO substrate at 5000 rpm for 60 s. After baking at 120 °C for one hour in an oven, the ITO substrates covered PEDOT−PSS were transferred into the glovebox. The active layer was deposited by spin coating at 800 rpm for 60 s in the glovebox. Finally, the cathodes of Ca (∼20 nm) and Al (∼110 nm) were deposited on the active layer by thermal evaporating. Performance of these solar cells was evaluated under A.M. 1.5 illumination (100 mW/cm^2) using a solar simulator (Abet Technologies, model no. 11000). In addition, we calculate the electron mobility by the space charge limited current (SCLC)

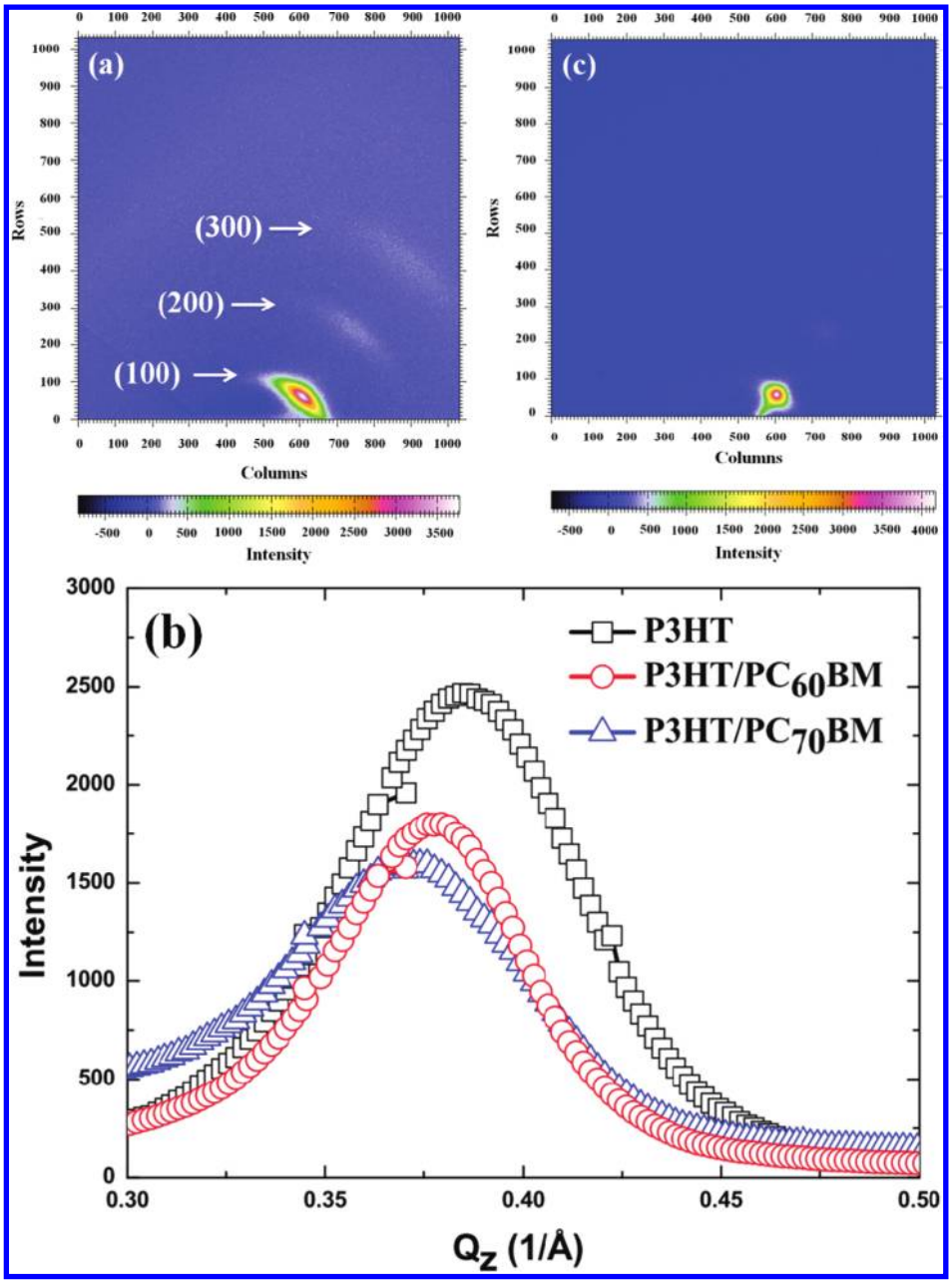

Figure 1. Out-of-plane GIWAXS 2D patterns of (a) pristine P3HT film and (c) P3HT/$PC_{70}BM$ film. (b) Reduced 1D GIWAXS profiles of pristine P3HT, P3HT/$PC_{60}BM$, and P3HT/$PC_{70}BM$ films.

model. The electron-only device was fabricated in the structure of Al/P3HT−PC_xBM/Al.

RESULTS AND DISCUSSION

First of all, we explore how the addition of different fullerene derivatives affects the crystalline behavior of P3HT by GIWAXS. The out-of-plane GIWAXS mainly comes from the oriented edge-on P3HT crystallites with lamellar ordered structure having (100) layers (stacking by polymer backbones) parallel to the substrate. Figure 1(a) clearly shows three strong reflection spots of pristine P3HT displayed on the GIWAXS 2D pattern. After P3HT was blended with either $PC_{60}BM$ or $PC_{70}BM$, the (100) reflection peak of the P3HT crystallites (edge-on type) varies in width. The full-width at half-maximum (fwhm) values of (100) peaks for pristine P3HT, P3HT/$PC_{60}BM$, and P3HT/$PC_{70}BM$ films are 0.073, 0.066, and 0.067 $Å^{-1}$, respectively, as shown in Figure 1(b). Figure 1(b) is the 1D GIWAXS profiles reduced along the z axis (out-of-plane direction) as a function of scattering vector (Q_z). According to the peak of pristine P3HT at $|Q_z| = 0.38$ $Å^{-1}$, the spacing of lamellar planes in these P3HT crystallites oriented along the z axis ([100] direction) can be estimated to be 16.7 Å. This value is consistent with literature data.[18] The slight shift of P3HT peak position in P3HT/$PC_{60}BM$ and P3HT/$PC_{70}BM$ films is found toward the low-Q region. The corresponding spacing of lamellar planes inside P3HT crystallites can be estimated to be 17.1 Å in P3HT/$PC_{60}BM$ film and 17.4 Å in P3HT/$PC_{70}BM$ film. According to a previous report,[34] the variation of lattice constant of P3HT would be stable when approaching high molecular weight (>30 000 g mol^{-1}). The molecular weight of P3HT used herein is very high, ∼ 61 881 g mol^{-1} with a low PDI of 1.48 and high regioregularity of 97.2%, and the

dx.doi.org/10.1021/jp210140j | J. Phys. Chem. C 2012, 116, 10238−10244

polymorphic factor due to the purity of polymer can be excluded. Therefore, we can deduce the spacing of lamellae changes roughly with the size of fullerene derivatives.

When the fullerene is mixed with P3HT followed by spin coating, there are phase separations occurred to form bulk heterojunction with P3HT-rich domains and fullerene-rich domains. Our previous study indicated that P3HT-rich domains are categorized into two types.[33] One is the network structure of PC_xBM molecules intercalated within the amorphous P3HT phase. The corresponding domain size can be characterized by GISAXS, as described in the later paragraphs. The other is the PC_xBM molecules intercalated around the boundary of the P3HT crystalline domain. We herein named the $PC_{60}BM$ intercalated around the P3HT crystalline domain as P3HT-crystal/$PC_{60}BM$ domain and $PC_{70}BM$ intercalated around the P3HT crystalline domain as P3HT-crystal/$PC_{70}BM$ domain. The corresponding crystal dimension D_z of edge-on P3HT crystallites for pristine P3HT, P3HT/$PC_{60}BM$ and P3HT/$PC_{70}BM$ films can be calculated to be 8.3 nm, 10.3 and 7.6 nm, respectively. But, the determined crystal size of P3HT in P3HT-crystal/$PC_{70}BM$ domain is of error due to the influence of high background from the low-Q region. It can be reasonably estimated that the crystal sizes of P3HT-crystal/$PC_{70}BM$ domain are similar to that of the P3HT-crystal/$PC_{60}BM$ domain after the subtraction of extrapolated background. Figure 1 (c) shows the evidence that the (200) and (300) reflection spots diminish due to the addition of $PC_{70}BM$. It suggests that the existence of fullerene molecules partially intercalated between the rims of P3HT lamellae layers interrupts the P3HT crystallization (polymer stacking). The relative crystallinity for P3HT/$PC_{60}BM$ and P3HT/$PC_{70}BM$ blend films is 36% and 32%, respectively, using the ratio of integrated area of (100) peak of the blend film to the pristine P3HT film (see Supporting Information, Figure S2). The results indicate the increased J_{sc} of P3HT/$PC_{70}BM$ blend films cannot be from its low crystallinity. Previous work[19] pointed out that the highly crystalline polymer solar cell with large crystal size has low performance because there is no sufficient intercalation of PCBM between side chains, leading to the poor PL quenching. In this study, the crystal sizes of ~10 nm are close to the diffusion length of exciton. Therefore, the charge separation in the 3D structure plays a major role in determining the PCE of a solar cell.

According to GIWAXS results, we have found the shift of (100) peak position in the P3HT-crystal/$PC_{70}BM$ domain toward the low-Q region is slight larger than that of the P3HT-crystal/$PC_{60}BM$ domain. The result reveals that a larger spacing of P3HT lamellae is formed in the P3HT-crystal/$PC_{70}BM$ domain due to the larger size of $PC_{70}BM$ and more $PC_{70}BM$ molecules partially intercalated between the rims of P3HT lamellar planes as compared with $PC_{60}BM$. The amount of fullerenes intercalated in different P3HT-crystal/PC_xBM domains is estimated quantitatively by GISAXS (described later), which is consistent with this result. Previous studies[19,20] showed that the intercalation of PCBM within the ordered PBTTT, PTT, and MDMO-PPV polymer crystals is favored under thermal equilibrium when the space between the side chains of polymer is large enough to accommodate a PCBM molecule. The interlayer spacing of PBTTT lamellar structure of ~30 Å has been deduced from the WAXS investigation that is corresponding to the length of two intercalated PCBM molecules between the layers of the polymer chain. We have used Material Studio software to calculate the size of fullerene derivatives to be in the range of ~15.0 Å (see Supporting Information, Figure S3). This size of fullerene derivative can be partially intercalated between the rims of (100) layers of lamellar structure of P3HT crystallites by slow evaporation of DCB solvent as indicated in our study. The GIWAXS data showed the interlayer spacing of P3HT is increased from 16.7 Å of pristine P3HT to 17.1 Å of P3HT/$PC_{60}BM$ and to 17.4 Å of P3HT/$PC_{70}BM$. We reasonably speculate the occurrence of intercalation of fullerene derivatives between the rims of (100) layers of P3HT lamella crystalline. Verploegen et al. reported the lamellar spacing of P3HT was increased from 16.68 Å of pristine P3HT film to 16.86 Å of P3HT/$PC_{60}BM$ (1:1) as the cast film and to 16.99 Å of P3HT/$PC_{60}BM$ (1:1) as the thermal annealed film at 220 °C for 10 min.[35] The slight increase of 0.18 and 0.31 Å are observed in the layer spacing by incorporation of $PC_{60}BM$ into P3HT without and with thermal annealing, respectively. Our results are consistent with this report showing the increase of 0.4 and 0.7 Å by incorporation of $PC_{60}BM$ and $PC_{70}BM$, respectively. The extent of increase of our samples actually is larger than that of the Verploegen et al. sample without annealing (0.18 vs 0.4 Å), which indicates the partial intercalation and side chain ordering happened simultaneously in our slow drying process. It is also interesting to note the extent of increase is much larger for $PC_{70}BM$ at 0.7 Å, which cannot explain only by its larger size. There should be much more $PC_{70}BM$ molecules to be intercalated around the boundary of P3HT crystallites due to its higher solubility.[27] Thus, the slight difference in the increase of the interlayer spacing of P3HT is very significant due to the occurrence of intercalation of fullerene derivatives into the rims of P3HT lamella crystalline for the blend of P3HT/PC_xBM. The schematics of the structures of P3HT-crystal/PC_xBM domains in P3HT/PC_xBM films are illustrated in Figure 2. The

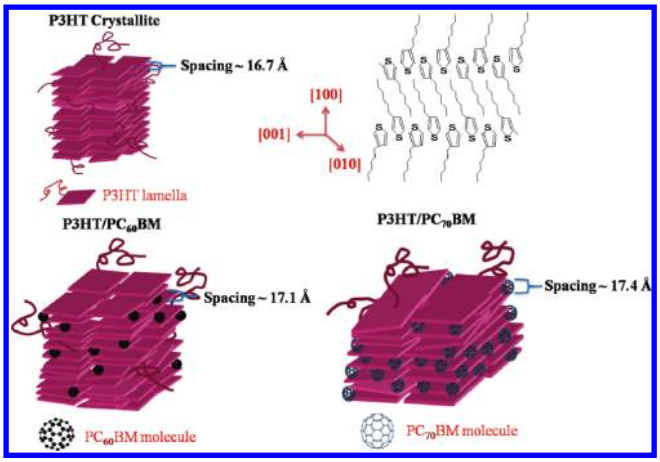

Figure 2. Schematics of (a) molecular-level structures for pristine and intercalated P3HT (the locally intercalated fullerene between the slightly disordered side chains) and (b) structures of P3HT-crystal/PC_xBM domains in P3HT/PC_xBM films.

distributional situation of $PC_{70}BM$ molecules around the boundary of P3HT crystallites generates more interfaces between P3HT and $PC_{70}BM$ that results in higher PCE of P3HT/$PC_{70}BM$ as compared with P3HT/$PC_{60}BM$. The recent study[36] reported that the PL spectrum of the P3HT/$PC_{70}BM$ blend is more largely quenched than that of the P3HT/$PC_{60}BM$ blend. Our GIWAXS result and the proposed model

dx.doi.org/10.1021/jp210140j | J. Phys. Chem. C 2012, 116, 10238–10244

provides the insight as the supplement of the structural interpretation regarding this PL result.

Figure 3 shows the in-plane GISAXS profiles of the P3HT/$PC_{60}BM$ and P3HT/$PC_{70}BM$ films with similar thickness of

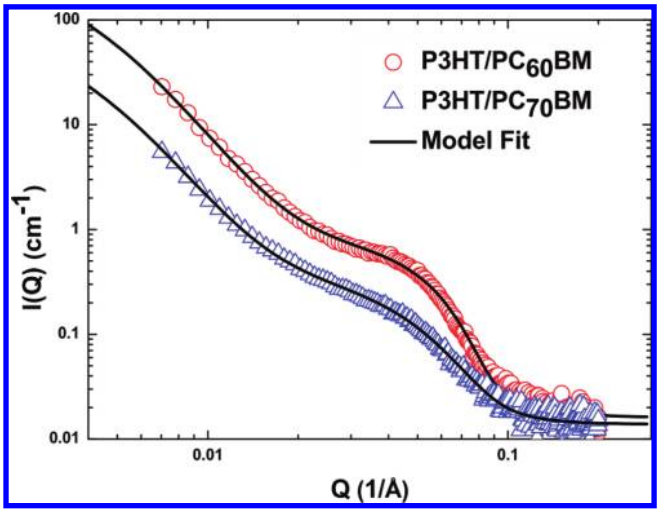

Figure 3. In-plane measured GISAXS profiles (as a function of scattering vector) of P3HT/$PC_{60}BM$ and P3HT/$PC_{70}BM$ films. The solid lines represent the SAXS intensities calculated by the DAB model.

~100 nm. According to our previous study,[33] the intensity upturn in the low-Q region (0.007 $Å^{-1}$ ~ 0.02 $Å^{-1}$) was attributed to the PC_xBM dispersed in the amorphous P3HT phase (i.e., the network structure formed by spatial distribution of PC_xBM molecules intercalated in the amorphous P3HT chains). We called this phase as the PC_xBM/P3HT amorphous domain. This upturn intensity can be fitted by using the Debye−Anderson−Brumberger (DAB) model with correlation length, ξ, for the characterization of the domains. The correlation lengths in the BHJ films of P3HT/$PC_{60}BM$ and P3HT/$PC_{70}BM$ are determined to be 23.7 and 25.3 nm, respectively. It indicates that the structures of PC_xBM/P3HT amorphous domains in both films are similar. The medium-Q and high-Q regions of GISAXS intensities are from the spherical clusters aggregated by PC_xBM molecules. As shown in Figure 3, the measured GISAXS profiles can be fitted well using the combination of the DAB model and the polydispersed spheres having Schultz size distribution with the hard-sphere interaction between PC_xBM clusters.[33] Moreover, the specific interface area, S_v, can be model-independently determined by the Porod law based on the GISAXS intensities in the high-Q region. S_v is the total interface area between the PC_xBM cluster and all the surrounding P3HT-related phases per unit of sample volume. It is especially worth noting that the S_v value is different from the interfacial area between PC_xBM and P3HT molecules in the P3HT-crystal/PC_xBM domain.

The structural parameters determined by the model-fitting, R, η, and p (radius, volume fraction, and polydispersity of size distribution of the PC_xBM cluster), for both blend films are summarized in Table 1. The radius and volume fraction of $PC_{60}BM$ clusters (R = 4.1 nm; η = 0.06) are significantly larger than those of $PC_{70}BM$ clusters (R = 3.2 nm; η = 0.02). The total volume fraction of $PC_{60}BM$ is similar to that of $PC_{70}BM$, which is based on the same weight ratio of PC_xBM to P3HT (1:1) used in film preparation. The low volume fraction of

Table 1. Structural Parameters Determined by the Model Fitting and Mode-Independent Porod-Law Methods for P3HT/$PC_{60}BM$ and P3HT/$PC_{70}BM$ Thin Films without Thermal Annealing

film	η (%)	R (nm)	p (polydis.)	ξ (nm)	S_v ($\times 10^{-3}$) ($Å^{-1}$)	$S_v/(\eta/R)$
P3HT/$PC_{60}BM$	6	4.1	0.12	23.7	2.7	1.8
P3HT/$PC_{70}BM$	2	3.2	0.24	25.3	1.0	1.6

$PC_{70}BM$ clusters is due to the higher solubility of $PC_{70}BM$ in DCB than that of $PC_{60}BM$. More $PC_{70}BM$ molecules tend to intercalate within P3HT crystallites, which lead to the reduction of aggregating into the $PC_{70}BM$ cluster. Furthermore, the specific interface areas (S_v) of $PC_{60}BM$ and $PC_{70}BM$ clusters in the blend films are model-independently determined to be 2.7 $\times$ 10^{-3} and 1.0 $\times$ 10^{-3} $Å^{-1}$. S_v data also show the evidence of the $PC_{60}BM$ cluster with higher volume fraction compared to that of the $PC_{70}BM$ cluster. According to the previous study and the values of the ratio of S_v to η/R (1.8 and 1.6, respectively, for P3HT/$PC_{60}BM$ and $PC_{70}BM$ blend films), it can be deduced that the partial attachment between fullerene clusters is occurred in both films.[33] The partial attachment of fullerene clusters is helpful for the construction of interpenetrating structure and efficient transport path for electron to electrode.

In order to correlate the nanostructure of BHJ with PCE, the performance of two solar cells fabricated from P3HT/$PC_{60}BM$ and P3HT/$PC_{70}BM$, respectively, were measured under simulated A.M. 1.5 illumination (100 mW/cm^2). These results are shown in Figure 4 and summarized in Table 2. The PCE of

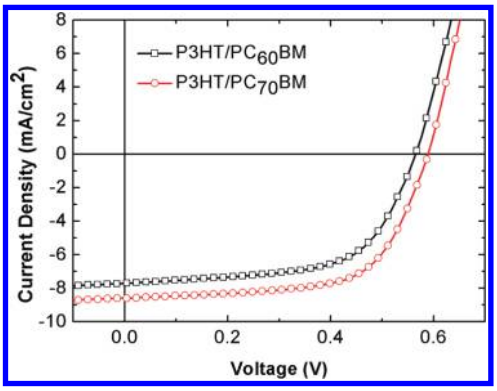

Figure 4. J−V characteristics of solar cells based on the P3HT/$PC_{60}BM$ and P3HT/$PC_{70}BM$ under A.M. 1.5 illumination (100 mW/cm^2).

Table 2. Performance of P3HT/$PC_{60}BM$ and P3HT/$PC_{70}BM$ Solar Cells without Thermal Annealing

device	Voc (V)	J_{sc} (mA/cm^2)	FF	PCE (%)
P3HT/$PC_{60}BM$	0.56	7.72	0.61	2.64
P3HT/$PC_{70}BM$	0.59	8.60	0.64	3.25

P3HT/$PC_{60}BM$ of 2.64% is lower than that of P3HT/$PC_{70}BM$ of 3.25%. The GISAXS analysis shows the volume fraction, specific interface area, and size of $PC_{60}BM$ clusters is higher than those of $PC_{70}BM$ clusters, leading to the more favorable electron transport. The electron mobility for the P3HT/$PC_{60}BM$ and P3HT/$PC_{70}BM$ films measured herein are 3.32 $\times$

dx.doi.org/10.1021/jp210140j | J. Phys. Chem. C 2012, 116, 10238−10244

10^{-4} and 1.66×10^{-4} $cm^2V^{-1}s^{-1}$, respectively. The result reflects the transport of charge carrier in the P3HT/PC_{60}BM film is better than that in the P3HT/PC_{70}BM film. It is also consistent with our structural characterization by using GISAXS, which showed the effectiveness of larger cluster size and higher volume fraction of PC_{60}BM clusters in the interpenetrating network of donor and acceptor phases. In contrast, the results of GIWAXS show that there are more PC_{70}BM molecules intercalated between the rims of the lamellar planes inside the P3HT-crystal/PC_{70}BM domain than PC_{60}BM. It implies that more interfaces between PC_{70}BM and P3HT are generated in P3HT/PC_{70}BM thin film. According to the previous study,[20] the increase of acceptor−donor interface in the P3HT-crystal/PC_{70}BM domain enhances the separation of charge carriers effectively.

The performance of a solar cell is mainly determined by the following parameters, including photon harvesting (light absorption and exciton generation), separation, and transport of charge carriers. Our result showed that the PCE of the P3HT/PC_{70}BM solar cell is better than that of the P3HT/PC_{60}BM solar cell mainly due to the improved short-circuit current. However, our measurements also show that both the electron mobility and phase-separated structures of polymer and fullerene as the transport path of charge carriers for the P3HT/PC_{70}BM solar cell are inferior to those of the P3HT/PC_{60}BM solar cell. Therefore, it can be evidenced that the light absorption, the subsequent exciton generation, and dissociation (charge separation) of the P3HT/PC_{70}BM solar cell should be superior to those of the P3HT/PC_{60}BM solar cell. Figure 5

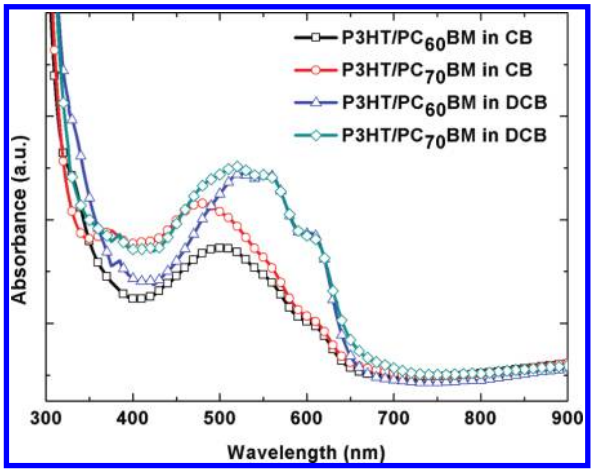

Figure 5. Absorption spectra of P3HT/PC_xBM for slow-drying (DCB) process and for relative fast-dry (CB) process.

shows the absorption spectra of P3HT/PC_xBM thin films prepared either by a slow-drying (DCB as solvent) process or a relative fast-drying (CB as solvent) process. The light harvesting is increased for slow-drying (DCB) samples as compared with that of relative fast-drying samples (CB), and a P3HT vibronic peak (~ 600 nm) is clearly observed for the slow-drying sample. It strongly supports our previous suggestion of improving ordering of P3HT side chains during the slow-drying process. For the slow-drying process, the P3HT/PC_{70}BM blend film exhibits stronger absorption in the visible wavelength range than that of P3HT/PC_{60}BM blend film due to PC_{70}BM molecules assisted ordering.[36] That results in increasing J_{sc} of the P3HT/PC_{70}BM solar cell. Moreover, we integrated the area of absorption spectra for P3HT/PC_xBM thin films in the region of 350~650 nm to show the increasing absorbance quantitatively. The absorption of the P3HT/PC_{70}BM blend film demonstrated an increase of 8.3% as compared with that of the P3HT/PC_{60}BM blend film. However, the J_{sc} of the P3HT/PC_{70}BM solar cell reveals an improvement of 11.4% compared with that of the P3HT/PC_{60}BM solar cell. Obviously, the improving J_{sc} is not entirely attributed to the increasing light absorption; molecular intercalation of fullerene plays a major role to enhance the J_{sc} of the P3HT/PC_{70}BM solar cell further. The effective exciton dissociation for the P3HT/PC_{70}BM solar cell is verified by our structural analysis. The enhanced exciton dissociation of the P3HT/PC_{70}BM blend film is resulted from the increasing interfacial area due to a high molecular intermixing between donor and acceptor. Therefore, we can conclude that the high PCE of the P3HT/PC_{70}BM solar cell is resulted from the following: (1) the enhanced light harvesting, and (2) effective charge carriers separated at the interface of PC_{70}BM-P3HT inside the P3HT-crystal/PC_{70}BM domain.

Generally speaking, it is hard to clarify how the critical steps, including charge separation, transport, and recombination, favor the PCE because of many variations in the processing and the complex nanostructure formation (from molecular level to nanoscale). By the combined GIWAXS/GISAXS measurements, electron mobility, absorption spectra, and PCE measurements, we can conclude that the nanostructure contributed by fullerene molecules intercalated with P3HT polymer plays an important role in the improvement of PCE in addition to the well-known PCBM cluster and pure P3HT crystallite. The size and volume fraction of the PC_xBM cluster/or aggregation treated with solvent annealing is usually lower than that of the PC_xBM cluster with thermal annealing.[33] This evidence can support this deduction about the importance of nanostructures formed by the PC_xBM molecules intercalated partially with P3HT polymer in BHJ when an annealing free process is employed.

CONCLUSION

We have quantitatively investigated various structures in the BHJ films of P3HT/PC_xBM to explore the effect of the type of fullerene derivatives on the phase separation driven by the slow-drying process without annealing. The present study demonstrates how the intercalation of fullerene around the domain of P3HT crystallites affects the self-organized nanostructures. The correlation between nanostructure and PCE is deduced according to combined GIWAXS/GISAXS measurements, electron mobility, absorption spectra, and PCE measurements. There are two kinds of nanostructure formation: (1) PC_xBM molecules partially intercalated between the rims of P3HT crystalline and in amorphous domains, and (2) aggregated PC_xBM clusters in PC_xBM domains during the slow-drying processing using different fullerene derivatives. The two nanostructures act as charge separation interfaces and charge transport paths in the solar cell. The PCE of the P3HT/PC_{70}BM solar cell is higher than that of P3HT/PC_{70}BM because the J_{sc} of the P3HT/PC_{70}BM solar cell is higher. The increased J_{sc} is resulted from the increased light harvesting and more efficient charge separation of effective molecular intermixing between P3HT and PC_{70}BM. A PCE of 3.25% has been reached for P3HT/PC_{70}BM solar cells without annealing.

dx.doi.org/10.1021/jp210140j | J. Phys. Chem. C 2012, 116, 10238−10244

■ ASSOCIATED CONTENT

Supporting Information

PEDOT−PSS effect on GISAXS and GIWAXS measurement, intensity variation in the incident angles of the GISAXS measurement, and calculated molecular size of fullerene and its derivative. This material is available free of charge via the Internet at http://pubs.acs.org.

■ AUTHOR INFORMATION

Corresponding Author

*E-mail: (C.-S. T.) cstsao@iner.gov.tw; (W.-F. S.) suwf@ntu.edu.tw.

Notes

The authors declare no competing financial interest.

■ ACKNOWLEDGMENTS

We would like to thank Mr. Wei-Ru Wu of the national synchrotron radiation research center (NSRRC) in Taiwan for the help in taking GISAXS data.

■ REFERENCES

(1) Park, S. H.; Roy, A.; Beaupré, S.; Cho, S.; Coates, N.; Moon, J. S.; Moses, D.; Leclerc, M.; Lee, K.; Heeger, A. J. *Nat. Photon.* **2009**, *3*, 297−302.
(2) Dennler, G.; Scharber, M. C.; Brabec, C. J. *Adv. Mater.* **2009**, *21*, 1323−1338.
(3) Moulé, A. J.; Meerholz, K. *Adv. Funct. Mater.* **2009**, *19*, 3028−3036.
(4) Kim, Y.; Cook, S.; Tuladhar, S. M.; Choulis, S. A.; Nelson, J.; Durrant, J. R.; Bradley, D. D. C.; Giles, M.; McCulloch, I.; Ha, C. S.; et al. *Nat. Mater.* **2006**, *5*, 197−203.
(5) Li, G.; Shrotriya, V.; Huang, J.; Yao, Y.; Moriarty, T.; Emery, K.; Yang, Y. *Nat. Mater.* **2005**, *4*, 864−868.
(6) van Bavel, S. S.; Sourty, E.; de With, G.; Loos, J. *Nano Lett.* **2008**, *9*, 507−513.
(7) Yang, X.; Loos, J.; Veenstra, S. C.; Verhees, W. J.; Wienk, M. M.; Kroon, J. M.; Michels, M. A. J.; Janssen, R. A. J. *Nano Lett.* **2005**, *5*, 579−583.
(8) Giridharagopal, R.; Ginger, D. S. *J. Phys. Chem. Lett.* **2010**, *1*, 1160−1169.
(9) Huang, Y. C.; Liao, Y. C.; Li, S. S.; Wu, M. C.; Chen, C. W.; Su, W. F. *Sol. Energy Mater. Sol. Cells* **2009**, *93*, 888−892.
(10) Padinger, F.; Rittberger, R. S.; Sariciftci, N. S. *Adv. Funct. Mater.* **2003**, *13*, 85−88.
(11) Huang, Y. C.; Chuang, S. Y.; Wu, M. C.; Chen, H. L.; Chen, C. W.; Su, W. F. *J. Appl. Phys.* **2009**, *106*, 034506.
(12) Li, G.; Yao, Y.; Yang, H.; Shrotriya, V.; Yang, G.; Yang, Y. *Adv. Funct. Mater.* **2007**, *17*, 1636−1644.
(13) Jo, J.; Kim, S. S.; Na, S. I.; Yu, B. K.; Kim, D. Y. *Adv. Funct. Mater.* **2009**, *19*, 866−874.
(14) Savenije, T. J.; Grzegorczyk, W. J.; Heeney, M.; Tierney, S.; McCulloch, I.; Siebbeles, L. D. A. *J. Phys. Chem. C* **2010**, *114*, 15116−15120.
(15) Chiu, M. Y.; Jeng, U. S.; Su, M. S.; Wei, K. H. *Macromolecules* **2010**, *43*, 428−432.
(16) Chiu, M. Y.; Jeng, U. S.; Su, C. H.; Liang, K. S.; Wei, K. H. *Adv. Mater.* **2008**, *20*, 2573−2578.
(17) Kiel, J. W.; Eberle, A. P. R; Mackay, M. E. *Phys. Rev. Lett.* **2010**, *105*, 168701.
(18) Singh, R. K.; Kumar, J.; Kumar, A.; Kumar, V.; Kant, R.; Singh, R. *Sol. Energy Mater. Sol. Cells* **2010**, *94*, 2386−2394.
(19) Mayer, A. C.; Toney, M. F.; Scully, S. R.; Rivnay, J.; Brabec, C. J.; Scharber, M.; Koppe, M.; Heeney, M.; McCulloch, I.; McGehee, M. D. *Adv. Funct. Mater.* **2009**, *19*, 1173−1179.
(20) Cates, N. C.; Gysel, R.; Beiley, Z.; Miller, C. E.; Toney, M. F.; Heeney, M.; McCulloch, I.; McGehee, M. D. *Nano Lett.* **2009**, *9*, 4153−4157.
(21) Tsao, C. S.; Yu, M. S.; Chung, T. Y.; Wu, H. C.; Wang, C. Y.; Chang, K. S.; Chen, H. L. *J. Am. Chem. Soc.* **2007**, *129*, 15997−16004.
(22) Chen, H. Y.; Hou, J.; Zhang, S.; Liang, Y.; Yang, G.; Yang, Y.; Yu, L.; Wu, Y.; Li, G. *Nat. Photon.* **2009**, *3*, 649−653.
(23) Liang, Y.; Xu, Z.; Xia, J.; Tsai, S. T.; Wu, Y.; Li, G.; Ray, C.; Yu, L. *Adv. Mater.* **2010**, *22*, E135−138.
(24) Chen, M. H.; Hou, J.; Hong, Z.; Yang, G.; Sista, S.; Chen, L. M.; Yang, Y. *Adv. Mater.* **2009**, *21*, 4238−4242.
(25) Hou, J.; Chen, H. Y.; Zhang, S.; Chen, R. I.; Yang, Y.; Wu, Y.; Li, G. *J. Am. Chem. Soc.* **2009**, *131*, 15586−15587.
(26) Boland, P.; Sunkavalli, S. S.; Chennuri, S.; Foe, K.; Abdel-Fattah, T.; Namkoong, G. *Thin Solid Films* **2010**, *518*, 1728−1731.
(27) Kadish, K. M.; Ruoff, R. S. *Fullerene: Chemistry, Physics and Technology*; Wiley: New York, 2002.
(28) Campoy-Quiles, M.; Ferenczi, T.; Agostineli, T.; Etchegoin, P. G.; Kim, Y.; Anthopoulos, T. D.; Stavrinou, P. N.; Bradley, D. D. C.; Nelson, J. *Nat. Mater.* **2008**, *7*, 158−164.
(29) Wang, T.; Pearson, A. J.; Lidzey, D. G.; Jones, R. A. L. *Adv. Funct. Mater.* **2011**, *21*, 1383−1390.
(30) Kim, K.; Liu, J.; Namboothiry, M. A. G.; Carroll, D. L. *Appl. Phys. Lett.* **2007**, *90*, 163511.
(31) Huang, Y. C.; Yen, W. C.; Liao, Y. C.; Yu, Y. C.; Hsu, C. C.; Ho, M. L.; Chou, P. T.; Su, W. F. *Appl. Phys. Lett.* **2010**, *96*, 123501.
(32) Wu, W. R.; Jeng, U. S.; Su, C. J.; Wei, K. H.; Su, M. S.; Chiu, M. Y.; Chen, C. Y.; Su, W. B.; Su, C. H.; Su, A. C. *ACS Nano* **2011**, *5*, 6233−6243.
(33) Liao, H. C.; Tsao, C. S.; Lin, T. H.; Chuang, C. M.; Chen, C. Y.; Jeng, U. S.; Su, C. H.; Chen, Y. F.; Su, W. F. *J. Am. Chem. Soc.* **2011**, *133*, 13064−13073.
(34) Zen, A.; Saphiannikova, M.; Dieter, N.; Grenzer, J.; Grigorian, S.; Pietsch, U.; Asawapirom, U.; Janietz, S.; Scherf, U.; Lieberwirth, I.; et al. *Macromolecules* **2006**, *39*, 2162−2171.
(35) Verploegen, E.; Mondal, R.; Bettinger, C. J.; Sok, S.; Toney, M. F.; Bao, Z. *Adv. Funct. Mater.* **2010**, *20*, 3519−3529.
(36) Zhang, F.; Zhuo, Z.; Zhang, J.; Wang, X.; Xu, X.; Wang, Z.; Xin, Y.; Wang, J.; Wang, J.; Tang, W.; et al. *Sol. Eng. Mater. Sol. Cells* **2011**, *97*, 71−77.